CHEMISTRY OF MATERIALS
Article

Chem. Mater. **2010,** *22,* 2093–2106 2093
DOI:10.1021/cm903495b

Green Dioxythiophene-Benzothiadiazole Donor−Acceptor Copolymers for Photovoltaic Device Applications

Pierre M. Beaujuge,[†] Jegadesan Subbiah,[‡] Kaushik Roy Choudhury,[‡] Stefan Ellinger,[†] Tracy D. McCarley,[§] Franky So,*[,‡] and John R. Reynolds*[,†]

[†]*The George and Josephine Butler Polymer Research Laboratory, Department of Chemistry, Center for Macromolecular Science and Engineering, University of Florida, Gainesville, Florida 32611,* [‡]*Department of Materials Science and Engineering, University of Florida, Gainesville, Florida 32611, and* [§]*Department of Chemistry, Louisiana State University, Baton Rouge, Louisiana 70803*

Received November 17, 2009. Revised Manuscript Received January 6, 2010

With the perspective of producing power-generating displays of various colors based on π-conjugated semiconducting polymers, we have developed a synthetic design aimed at addressing color states commonly difficult to attain. Herein, we report on the structure−property relationships and performance in photovoltaic devices of a series of green-colored donor−acceptor (DA) π-conjugated polymers comprised of electron-rich 3,4-dioxythiophenes (DOTs) and the electron-deficient 2,1,3-benzothiadiazole (BTD). In particular, the synthesis and chemical polymerization of two DOT-BTD regiosymmetric oligomers (pentamers **M2** and **M3**), that can be chemically oxidized to yield two-band absorbing polymers with a transmission window in the 480−560 nm range hence reflecting/transmitting the color green (**P2** and **P3**), is reported. The optical and electrochemical properties of **P2** and **P3** are described and compared to those of a blue-colored parent polymer (**P1**) obtained via the polymerization of a smaller DOT-BTD oligomeric precursor (trimer **M1**). The photovoltaic (PV) properties of **P1**−**P3** were investigated in DA bulk heterojunction (BHJ) devices with $PC_{60}BM$ as the acceptor. **P2** and **P3** afforded green-colored devices with up to 1.9% power conversion efficiency (PCE) under AM 1.5 G solar illumination. Taking into account the differences in polymer energy band structure, we have replaced PEDOT:PSS by MoO_3 and optimized the solar-cell device configuration for the most efficient polymer derivative (**P3**), demonstrating up to a 2.71% PCE. Insight into the morphology and charge transport of these polymers in blends with PCBM is provided and related to the synthetic design and PV device performance.

1. Introduction

As first described by Heeger et al. in 1995,[1] interpenetrating networks of semiconducting polymers and fullerene derivatives, namely bulk heterojunctions (BHJs), have rapidly become the cornerstone of organic solar cell development, promising higher densities of photogenerated charges, more effective charge extraction, and cost-effective solution processing. While power conversion efficiencies as high as 10% in single junction solar cells[2] and 15% in tandem devices[3] have been anticipated, the highest reported values surprisingly remain in the 5−6% range,[4−7] with the exception of a few recent contributions reporting higher efficiencies.[8−10] Of all the variables influencing BHJ device performance, the polymer's energy band structure determines the width of the spectral absorption, impacts the device open-circuit voltage (V_{OC}), and controls the photoinduced electron transfer to the strongly accepting fullerene analogue. To this end, the donor−acceptor (DA) approach, introduced by Havinga et al. in macromolecular systems[11] via alternating electron-rich and electron-poor substituents along a conjugated backbone, has attracted a good deal of attention in recent years. Thereby, a number of narrow-bandgap π-conjugated polymers absorbing at longer wavelengths than wide-bandgap all-donor parents (e.g., P3HT, MEH-PPV, and MDMO-PPV) have been synthesized.[7,12−18] Low-bandgap polymers for photovoltaic (PV) applications

*Corresponding author e-mail: reynolds@chem.ufl.edu (J.R.R.); fso@mse.ufl.edu (F.S.).

(1) Yu, G.; Gao, J.; Hummelen, J. C.; Wudl, F.; Heeger, A. J. *Science* **1995**, *270*, 1789.
(2) Scharber, M. C.; Mühlbacher, D.; Koppe, M.; Denk, P.; Waldauf, C.; Heeger, A. J.; Brabec, C. J. *Adv. Mater.* **2006**, *18*, 789.
(3) Dennler, G.; Scharber, M. C.; Ameri, T.; Denk, P.; Forberich, K.; Waldauf, C.; Brabec, C. J. *Adv. Mater.* **2008**, *20*, 579.
(4) Thompson, B. C.; Fréchet, J. M. J. *Angew. Chem., Int. Ed.* **2008**, *47*, 58.
(5) Zhang, Y.; Cai, X.; Bian, Y.; Li, X.; Jiang, J. *J. Phys. Chem. C* **2008**, *112*, 5148.
(6) Gunes, S.; Neugebauer, H.; Sariciftci, N. S. *Chem. Rev.* **2007**, *107*, 1324.
(7) Hou, J.; Chen, H.-Y.; Zhang, S.; Li, G.; Yang, Y. *J. Am. Chem. Soc.* **2008**, *130*, 16144.
(8) Hou, J.; Chen, H.-Y.; Zhang, S.; Chen, R. I.; Yang, Y.; Wu, Y.; Li, G. *J. Am. Chem. Soc.* **2009**, *131*, 15586.
(9) Chen, H.-Y.; Hou, J.; Zhang, S.; Liang, Y.; Yang, G.; Yang, Y.; Yu, L.; Wu, Y.; Li, G. *Nat. Photon.* **2009**, *3*, 649.
(10) Park, S. H.; Roy, A.; Beaupre, S.; Cho, S.; Coates, N.; Moon, J. S.; Moses, D.; Leclerc, M.; Lee, K.; Heeger, A. J. *Nat. Photon.* **2009**, *3*, 297.
(11) Havinga, E. E.; Hoeve, W.; Wynberg, H. *Synth. Met.* **1993**, *55*, 299.
(12) Wienk, M. M.; Turbiez, M.; Janssen, R. A. J. *Adv. Mater.* **2008**, *20*, 2556.

Published on Web 02/04/2010

have also recently been highlighted and reviewed by a number of research groups.[4,6,19−25]

With the concept of bandgap-engineering comes the idea that various colors can subsequently be accessed and taken advantage of. For example, in recent years, the DA approach has proven particularly useful in the synthesis of nonemissive polymer electrochromes, extending the palette of colors available for electrochromic display technologies.[26,27] On the other hand, solution-processed organic electronics suitable for combined photovoltaic/display devices, power-generating units (such as photovoltaic plants and trees) or light-harvesting window applications, are now emerging. An essential step forward in this area consists of developing new synthetic strategies which take both bandgap/color-engineering and the enhancement of the polymer charge transport into account simultaneously. While dye-sensitized solar cells of practically any color can be made based on the use of small molecules,[28−30] the most established photovoltaic polymers commonly yield red (e.g., P3HT),[31] orange (e.g., MDMO- or MEH-PPV),[20] or blue (e.g., PCPDTBT)[13] light-harvesting modules. In particular, only a few recent reports have addressed the use of neutral state green polymers in semiconducting polymer solar cells (PSCs), yet without addressing the rationale relative to the color obtained.[17,32] In fact, the color green is not readily accessible in π-conjugated polymers as the backbone has to be carefully designed to exhibit a two-band absorption in the visible with a window of transmission centered in the 490−560 nm region of the spectrum.[26,33,34] Though structure−property correlation studies can help establish parallels and trends between molecular structure, color, charge transport, and PV performance, efforts describing a specific polymer design and the rationale that led to it remains limited.

Janssen et al. have described the performance of a branched alkyl-substituted dioxythiophene- and 2,1,3-benzothiadiazole-containing copolymer (control polymer **P1** in this manuscript) in BHJ solar cells with $PC_{60}BM$ ([6,6]-phenyl-C61 butyric acid methyl ester).[35] This low bandgap derivative (~1.55 eV) exhibited a spectral response extending from 350 to 800 nm, along with a fill factor (FF) of 42% and an overall PCE of 0.9% under AM 1.5 at optimized polymer:PCBM composition. Importantly, while the polymer showed a relatively high open-circuit voltage of 0.77 V, the external quantum efficiency (EQE) remained low (maxima of 20% at ~450 nm and 13% at ~630 nm), hence suggesting a charge-transport limited device performance. In comparison, Krebs et al. for example have carefully explored semiconducting copolymers combining alkyl-substituted thiophene building units and 2,1,3-benzothiadiazole, reporting up to 1% of PCE in conventional solar cell device architectures.[18,36,37]

In this contribution, we report on the synthesis, optical, and electrochemical characterization, and photovoltaic performance of a series of dioxythiophene-benzothiadiazole (DOT-BTD) copolymers designed to provide insight into how careful structural modifications can be used to enhance the charge transport properties and photovoltaic response of DA π-conjugated polymers. Using the DOT-BTD polymer platform separately developed by Janssen et al. for solar cells and by Reynolds et al. for electrochromic applications (see Figure 1), we demonstrate how the polymer optical absorption can be designed to transmit 480−560 nm light (hence reflecting/transmitting the color green), and how its charge transport properties can be simultaneously optimized to improve the polymer EQE and, in turn, its PCE via the increase of photogenerated current (J_{SC}).

2. Experimental Section

2.1. Materials and Methods. All reagents were purchased from commercial sources and used without further purification, unless otherwise noted. We have previously reported the syntheses of **M1**, **M1′**, and **P1**.[38] The solvents were distilled and dried using known methods.[39] All reactions were carried under argon atmosphere unless otherwise mentioned. ^{1}H NMR and ^{13}C NMR spectra were collected on a Mercury 300 MHz using $CDCl_3$ and were referenced to the solvent residual peak ($CDCl_3$: ^{1}H: δ = 7.26 ppm, ^{13}C: δ = 77.23 ppm). Elemental analyses were carried out by Atlantic Microlab, Inc. High resolution mass

(13) Mühlbacher, D.; Scharber, M.; Morana, M.; Zhu, Z.; Waller, D.; Gaudiana, R.; Brabec, C. *Adv. Mater.* **2006**, *18*, 2884.
(14) Kim, J. Y.; Lee, K.; Coates, N. E.; Moses, D.; Nguyen, T.-Q.; Dante, M.; Heeger, A. J. *Science* **2007**, *317*, 222.
(15) Ergang, W.; Li, W.; Linfeng, L.; Chan, L.; Wenliu, Z.; Junbiao, P.; Yong, C. *Appl. Phys. Lett.* **2008**, *92*, 033307.
(16) Blouin, N.; Michaud, A.; Gendron, D.; Wakim, S.; Blair, E.; Neagu-Plesu, R.; Belletete, M.; Durocher, G.; Tao, Y.; Leclerc, M. *J. Am. Chem. Soc.* **2008**, *130*, 732.
(17) Svensson, M.; Zhang, F.; Veenstra, S. C.; Verhees, W. J. H.; Hummelen, J. C.; Kroon, J. M.; Inganäs, O.; Andersson, M. R. *Adv. Mater.* **2003**, *15*, 988.
(18) Bundgaard, E.; Krebs, F. C. *Macromolecules* **2006**, *39*, 2823.
(19) Li, Y.; Zou, Y. *Adv. Mater.* **2008**, *20*, 2952.
(20) Dennler, G.; Scharber, M. C.; Brabec, C. J. *Adv. Mater.* **2009**, *21*, 1323.
(21) Winder, C.; Sariciftci, N. S. *J. Mater. Chem.* **2004**, *14*, 1077.
(22) Bundgaard, E.; Krebs, F. C. *Sol. Energy Mater. Sol. Cells* **2007**, *91*, 954.
(23) Kroon, R.; Lenes, M.; Hummelen, J. C.; Blom, P. W. M.; de Boer, B. *Polym. Rev.* **2008**, *48*, 531.
(24) Helgesen, M.; Sondergaard, R.; Krebs, F. C. *J. Mater. Chem.* **2010**, *20*, 36.
(25) Chen, J.; Cao, Y. *Acc. Chem. Res.* **2009**, *42*, 1709.
(26) Sonmez, G.; Shen, C. K. F.; Rubin, Y.; Wudl, F. *Angew. Chem., Int. Ed.* **2004**, *43*, 1498.
(27) Sonmez, G. *Chem. Commun.* **2005**, 5251.
(28) Gledhill, S. E.; Scott, B.; Gregg, B. A. *J. Mater. Res.* **2005**, *20*, 3167.
(29) Kong, F.-T.; Dai, S.-Y.; Wang, K.-J. *Adv. OptoElectron.* **2007**, *2007*, 1.
(30) Gratzel, M. *J. Photochem. Photobiol., A.* **2004**, *164*, 3.
(31) Huang, J.; Li, G.; Yang, Y. *Adv. Mater.* **2008**, *20*, 415.
(32) Zhang, F.; Jespersen, K. G.; Björström, C.; Svensson, M.; Andersson, M. R.; Sundström, V.; Magnusson, K.; Moons, E.; Yartsev, A.; Inganäs, O. *Adv. Funct. Mater.* **2006**, *16*, 667.
(33) Asuman, D.; Gunbas, G. E.; Camurlu, P.; Toppare, L. *Chem. Commun.* **2007**, 3246.
(34) Beaujuge, P. M.; Ellinger, S.; Reynolds, J. R. *Adv. Mater.* **2008**, *20*, 2772.
(35) Wienk, M. M.; Struijk, M. P.; Janssen, R. A. J. *Chem. Phys. Lett.* **2006**, *422*, 488.
(36) Bundgaard, E.; Krebs, F. C. *Sol. Energy Mater. Sol. Cells* **2007**, *91*, 1019.
(37) Bundgaard, E.; Shaheen, S. E.; Krebs, F. C.; Ginley, D. S. *Sol. Energy Mater. Sol. Cells* **2007**, *91*, 1631.
(38) Beaujuge, P. M.; Ellinger, S.; Reynolds, J. R. *Nat. Mater.* **2008**, *7*, 795.
(39) Armarego, W. L. F.; Chai, C. L. L. *Purification of Laboratory Chemicals*, 5th ed.; Elsevier: 2003.

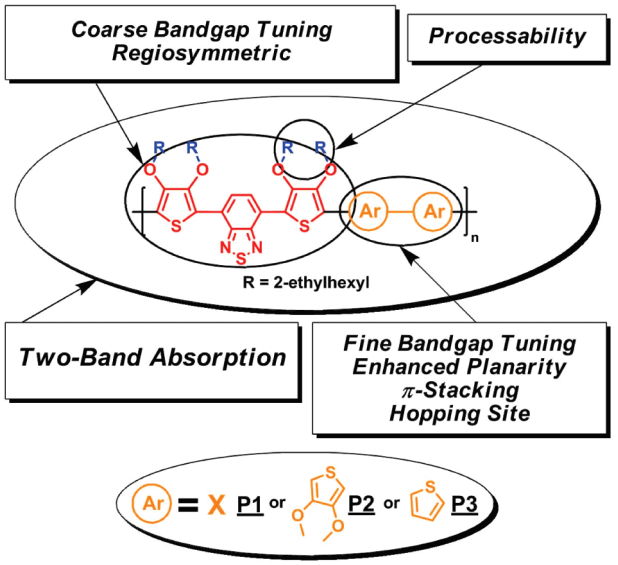

Figure 1. Designing dioxythiophene-benzothiadiazole (DOT-BTD) donor–acceptor copolymers with tunable absorption spectra and charge transport properties. (Figure 1 was adapted with permission from *ACS Appl. Mater. Interfaces* **2009**, *1*, 1154–1158. Copyright 2009 American Chemical Society).

spectrometry was performed by the spectroscopic services at the Department of Chemistry of the University of Florida with a Finnigan MAT 96Q mass spectrometer. MALDI mass spectra were acquired in linear and reflectron mode in the Department of Chemistry at LSU using a Bruker ProFlex III mass spectrometer. Gel permeation chromatography (GPC) was performed using a Waters Associates GPCV2000 liquid chromatography system with its internal differential refractive index detector (DRI) at 40 °C, using two Waters Styragel HR-5E columns (10 μm PD, 7.8 mm i.d., 300 mm length) with HPLC grade THF as the mobile phase at a flow rate of 1.0 mL/min. Injections were made at 0.05–0.07% w/v sample concentration using a 220.5 μL injection volume. Retention times were calibrated against narrow molecular weight polystyrene standards (Polymer Laboratories; Amherst, MA). Electrochemistry was performed using a single compartment three-electrode cell, a Pt flag as the counter electrode, a silver wire pseudoreference electrode calibrated using a 5 mM solution of Fc/Fc^+ in 0.1 M TBAP/propylene carbonate (PC) electrolyte solutions, and a platinum disk (0.02 cm^2) as the working electrode. An EGG Princeton Applied Research model 273A potentiostat/galvanostat was used under the control of Corrware II software from Scribner and Associates. Electrochemical measurements were carried out in an argon-filled drybox (Vacuum Atmospheres). All absorption spectra were collected using a Varian Cary 500 UV–vis-NIR spectrophotometer. Polymer solar cell devices were processed on prepatterned ITO-coated glass substrates with a sheet resistance of 20 Ω/cm^2. First, a thin layer (30 nm) of PEDOT:PSS (Baytron AI4083 from HC Starck) was spin-coated on ITO-coated substrates, followed by spin coating of a mixed solution of polymer (4 mg/mL) and PCBM (99% pure, Solenne BV) in chlorobenzene. Alternatively, a MoO_3 interlayer (10 nm) was thermally evaporated on the precleaned ITO substrate under a vacuum of 10^{-6} torr. The polymer:PCBM solution in chlorobenzene was stirred at room temperature for 16 h, filtered, and spin-coated. After the active layer was cast, it was subjected to a thermal annealing step of 70 °C for 45 min. LiF (1 nm) and aluminum (100 nm) were thermally evaporated at a vacuum of $\sim 10^{-6}$ mbar on top of polymer:PCBM active layer. The area of each device pixel is 0.04 cm^2. Current density versus voltage measurements were carried out using a Keithley 4200 semiconductor characterization system under AM1.5G, 100 mW/cm^2 illumination from a 150 W ozone free xenon arc lamp (Newport). The Newport 70260 radiant power meter in conjunction with a Newport 70268 probe was used to measure the power densities of the white-light illumination. National Institute of Standards and Technology (NIST) calibrated UV-enhanced silicon, and germanium photodetectors were used to calibrate the measurements. Device fabrication was performed under nitrogen atmosphere, and characterizations were performed in air without encapsulation. Hole-only devices: either solutions of pristine polymers (P1, P2, P3) in chlorobenzene (16 mg mL^{-1}) or polymer:PCBM mixed solution (as used for solar cells) were employed. Pd (as opposed to Au, for reasons outlined later in this manuscript) was thermally deposited to serve as the top counter electrode. Surface morphology characterization: AFM in tapping mode (Dimension 3100, Digital Instruments), Si AFM tip with a force constant of 40 N m^{-1}.

2.2. Synthesis of Macromonomer M2. Macromonomer **M1′** (1.3 g, 1.08 mmol), 3,4-dimethoxythiophen-2-yl)-trimethylstannane (1.55 g, 5.04 mmol), and $Pd(PPh_3)_2Cl_2$ (4 mol %) were cycled (argon/vacuum, 3×) and subsequently dissolved in 30 mL of THF. The mixture was stirred for 24 h at 60 °C, the solvent was evaporated, and the product was purified by column chromatography on silica with hexane/dichloromethane (1:1) as the eluent. The solvent was evaporated, and **M2** was obtained as a purple-blue tacky solid (0.97 g, 43%). ^{1}H NMR (300 MHz, $CDCl_3$) δ = 8.30 (s, 2H), 6.18 (s, 2H), 4.06 (d, J = 6.6 Hz, 4H), 3.98 (s, 6H), 3.93 (m, 4H), 3.87 (s, 6H), 2.00–1.10 (m, 36H), 1.00–0.79 (m, 24H); ^{13}C NMR (75 MHz, $CDCl_3$) δ = 153.07, 150.60, 148.39, 146.36, 143.46, 128.02, 124.65, 119.48, 117.70, 95.43, 76.61, 60.40, 57.46, 40.54, 40.48, 34.89, 31.82, 30.51, 29.30, 25.51, 23.86, 23.77, 23.40, 23.30, 22.88, 20.92, 14.37, 14.35, 14.27, 11.36, 11.23. HRMS (TOF) [MH^+] m/z calcd. for $C_{58}H_{84}N_2O_8S_5$: 1097.4904 Found: 1097.4948. Anal. Calcd. for $C_{58}H_{84}N_2O_8S_5$: C 63.47, H 7.71, N 2.55 Found: C 64.03, H 7.89, N 2.56.

2.3. Synthesis of Macromonomer M3. Macromonomer **M1′** (1.4 g, 1.44 mmol), tributyl(thiophen-2-yl)stannane (1.61 g, 4.32 mmol), and $Pd(PPh_3)_2Cl_2$ (4 mol %) were cycled (argon/vacuum, 3×) and subsequently dissolved in 30 mL of THF. The mixture was stirred for 24 h at 60 °C, the solvent was evaporated, and the product was purified by column chromatography on silica with hexane/dichloromethane (3:1) as the eluent. The solvent was evaporated, and **M3** was obtained as a purple tacky solid (0.72 g, 51%). ^{1}H NMR (300 MHz, $CDCl_3$) δ = 8.41 (s, 2H), 7.39 (dd, J = 1.2, 2.4 Hz, 2H), 7.31 (dd, J = 1.2, 3.9 Hz, 2H), 7.07 (dd, J = 3.6, 1.5 Hz, 2H), 4.05–3.97 (m, 8H), 1.91–1.22 (m, 36H), 1.00–0.81 (m, 24H); ^{13}C NMR (75 MHz, $CDCl_3$) δ = 152.85, 149.23, 145.99, 134.81, 127.74, 127.17, 125.29, 124.23, 123.98, 122.21, 118.45, 76.66, 40.61, 40.55, 30.52, 29.33, 23.86, 23.37, 23.31, 14.35, 14.28, 11.36, 11.27. HRMS (TOF) [MH^+] m/z calcd. for $C_{54}H_{76}N_2O_4S_5$: 977.4481 Found: 977.4456. Anal. Calcd. for $C_{54}H_{76}N_2O_4S_5$: C 66.35, H 7.84, N 2.87 Found: C 67.10, H 7.93, N 2.94.

2.4. Synthesis of Polymer P2. Macromonomer **M2** (260 mg, 0.24 mmol) was dissolved in chloroform (25 mL). A solution of anhydrous $FeCl_3$ (195 mg, 1.2 mmol, 5eq) in nitromethane was added dropwise over a period of 45 min to the stirred monomer at room temperature (the dark purple monomer solution turned progressively dark blue-green with addition of oxidizing agent). The mixture was stirred 24 h at room temperature. It was then precipitated into methanol (200 mL). The precipitate was

Scheme 1

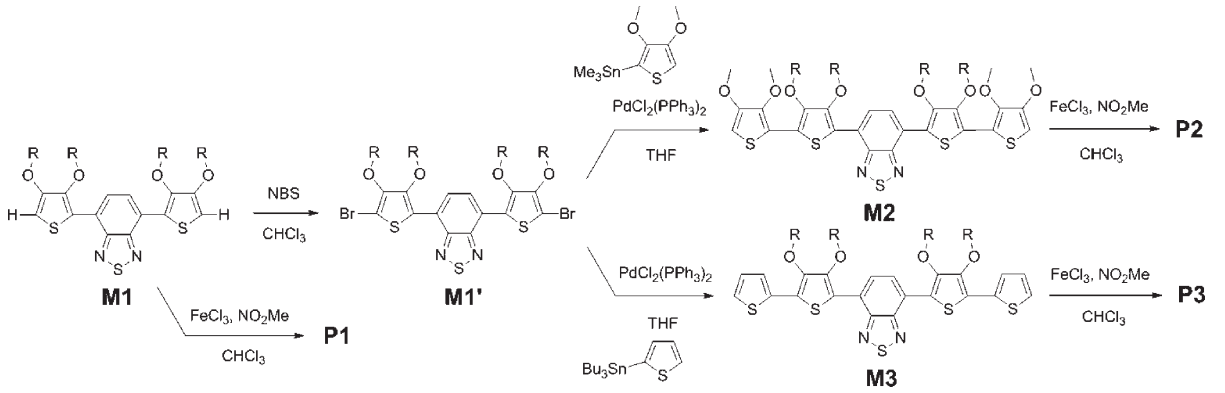

filtered, redissolved in chloroform (200 mL), and stirred for 3 h with hydrazine monohydrate (6 mL). After evaporation, the concentrate (dark blue-green) was precipitated into methanol (200 mL), and the precipitate was filtered through a Soxhlet thimble and purified via Soxhlet extraction for 24 h with methanol. The polymer was extracted with chloroform, concentrated by evaporation, precipitated in methanol (200 mL), and collected as a dark solid (220 mg, 85%). ^{1}H NMR (300 MHz, $CDCl_3$) δ = 8.33 (bs, 2H), 4.2−3.8 (br, 20H), 2.0−1.1 (br, 36H), 1.1−0.7 (br, 24H). GPC analysis: M_n = 43 000 g mol^{-1}, M_w = 88 600 g mol^{-1}, PDI = 2.1. Anal. Calcd. for $C_{54}H_{72}N_2O_4S_5$ C 63.58, H 7.54, N 2.56 Found: C 64.68, H 7.69, N 2.53.

2.5. Synthesis of Polymer P3. Macromonomer **M3** (300 mg, 0.307 mmol) was dissolved in chloroform (50 mL). A solution of anhydrous $FeCl_3$ (248 mg, 1.53 mmol, 5eq) in nitromethane was added dropwise over a period of 45 min to the stirred monomer at room temperature (the dark purple monomer solution turned progressively dark blue-green with addition of oxidizing agent). The mixture was stirred 24 h at room temperature. It was then precipitated into methanol (200 mL). The precipitate was filtered, redissolved in chloroform (200 mL), and stirred for 3 h with hydrazine monohydrate (6 mL). After evaporation, the concentrate (dark blue-green) was precipitated into methanol (200 mL), and the precipitate was filtered through a Soxhlet thimble and purified via Soxhlet extraction for 24 h with methanol. The polymer was extracted with chloroform, concentrated by evaporation, precipitated in methanol (200 mL), and collected as a dark solid (145 mg, 48%). ^{1}H NMR (300 MHz, $CDCl_3$) δ = 8.44 (bs, 2H), 7.5−7.0 (br, 4H), 4.3−3.8 (br, 8H), 2.0−1.1 (br, 36H), 1.1−0.7 (br, 24H). GPC analysis: M_n = 69 300 g mol^{-1}, M_w = 111 600 g mol^{-1}, PDI = 1.6. Anal. Calcd. for $C_{54}H_{74}N_2O_4S_5$ C 66.49, H 7.65, N 2.87 Found: C 66.69, H 7.67, N 2.77.

3. Results and Discussion

3.1. Synthetic Design and Polymer Synthesis. While using the donor−acceptor approach in the context of soluble electrochromic (EC) polymer design, we have recently demonstrated that color states commonly difficult to achieve in π-conjugated polymers, such as greens of tunable hues, could be achieved relying on a two-band absorption in the visible attainable on the basis of a linear combination of well-chosen electron-rich (donor) and electron-deficient (acceptor) building units.[40] Wudl et al. had alternatively created dual visible absorptions by introducing a secondary chromophore in broken conjugation with the polymer main-chain.[26] More recently, we have further shown how varying the concentration and distribution of electron-rich and -poor moieties incorporated in the polymer repeat unit impacts the polymer two-band absorption, adjusting the relative intensities and overlap of the two optical transitions as the donor-to-acceptor ratio changes.[38] Throughout both studies, a number of symmetrical dioxythiophene-benzothiadiazole (DOT-BTD) based conjugated oligomers exhibiting low oxidation potentials were synthesized and oxidatively polymerized to yield polymers having number average molecular weights ranging from 10 to 48 kDa depending on the nature of the DOT incorporated and the size of the macromonomers polymerized. As the polymer structures were successfully confirmed, we realized that this approach could be employed to produce high molecular weight polymers for organic solar cells, possessing repeat units otherwise synthetically difficult to obtain via conventional Pd-mediated polycondensation techniques.

Since solution-processable polymers specifically designed for EC applications generally incorporate a large number of appended solubilizing side chains, they do not commonly show a pronounced degree of order or π-stacking, and their charge transport properties tend to be modest.[41−43] In contrast, in addition to the requirement for a broad spectral absorption across the visible and near-IR, conjugated polymers suitable for BHJ applications with PCBM must exhibit balanced charge-carrier mobilities over the polymer- and PCBM-rich phases (less than 2 orders of magnitude difference) to avoid falling into a space-charge limited device performance regime. Considering that pendant-groups alter the planarity,[44−46] macroscopic organization,[47] and intermolecular

(40) Beaujuge, P. M.; Pisula, W.; Tsao, H. N.; Ellinger, S.; Müllen, K.; Reynolds, J. R. *J. Am. Chem. Soc.* **2009**, *131*, 7514.
(41) Thompson, B. C.; Kim, Y. G.; McCarley, T. D.; Reynolds, J. R. *J. Am. Chem. Soc.* **2006**, *128*, 12714.
(42) Galand, E. M.; Kim, Y.-G.; Mwaura, J. K.; Jones, A. G.; McCarley, T. D.; Shrotriya, V.; Yang, Y.; Reynolds, J. R. *Macromolecules* **2006**, *39*, 9132.
(43) Campos, L. M.; Mozer, A. J.; Günes, S.; Winder, C.; Neugebauer, H.; Sariciftci, N. S.; Thompson, B. C.; Reeves, B. D.; Grenier, C. R. G.; Reynolds, J. R. *Sol. Energy Mater. Sol. Cells* **2006**, *90*, 3531.
(44) McCullough, R. D.; Lowe, R. D. *J. Chem. Soc., Chem. Commun.* **1992**, *1*, 70.
(45) McCullough, R. D.; Lowe, R. D.; Jayaraman, M.; Anderson, D. L. *J. Org. Chem.* **1993**, *58*, 904.
(46) SanMiguel, L.; Matzger, A. J. *Macromolecules* **2007**, *40*, 9233.

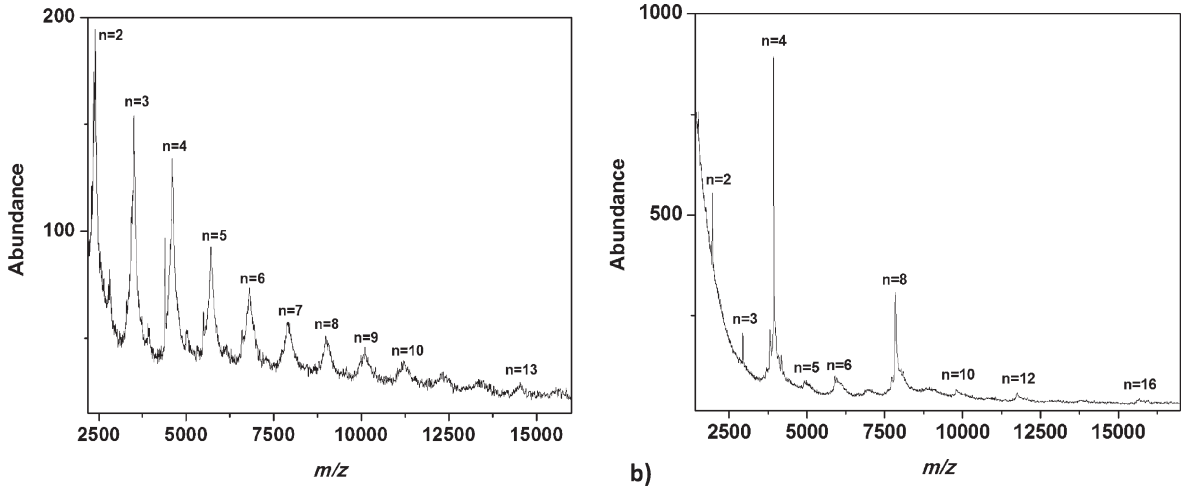

Figure 2. MALDI-MS of DA-copolymers **a) P2** and **b) P3**. DCTB was used as the matrix in each case.

distances[48] in π-conjugated polymers, we have designed two repeat units with minimal extent of solubilizing groups, as evidenced by **M2** and **M3** in Scheme 1. Scheme 1 further illustrates the synthetic pathways leading to copolymers **P1**−**P3**. Here, the acceptor BTD was first symmetrically functionalized with two electron-rich 3,4-disubstituted 2-ethylhexyloxythiophenes to yield the intermediate **M1** (bright orange oil). The macromonomers **M2** and **M3** were then accessed via traditional Stille couplings[49] between the halogenated precursor **M1′** and the tin-functionalized 3,4-dimethoxythiophene and unsubstituted thiophene, respectively. **M2** and **M3** were purified by column chromatography over silica using mixtures of hexanes and dichloromethane and isolated as tacky solids. **P2** and **P3** were subsequently polymerized from **M2** and **M3** using the mild oxidizing agent $FeCl_3$, and the oxidized polymers were reduced with hydrazine. In **P2** and **P3**, the DOTs bearing the solubilizing side chains are spaced by conjugated bridges composed of two heterocycles with either short pendant groups (**P2**) or no substituent (**P3**), hence progressively maximizing the backbone planarity in comparison with the control polymer **P1** obtained from the self-condensation of **M1**. In fact, it is expected that the steric hindrance associated with the in-plane branched alkoxy substituents of **P1** twists two adjacent DOT units out of planarity, hence reducing the polymer conjugation length considerably. In the meanime, lowering the concentration of solubilizing groups to the necessary extent to retain solubility as in **P2** and **P3** should reduce the chain-to-chain distances (or lamellar spacing), promote π-stacking interactions, and, in turn, enhance charge transport in the corresponding materials.[50−52]

Importantly, the donor−acceptor character of the pentameric structures **M2** and **M3** was anticipated to retain the polymer two-band absorption in the visible required to set the color green previously obtained for the polymer electrochrome.

It is worth noting that **P1** has first been produced by Janssen and colleagues via a nickel-catalyzed Yamamoto polycondensation procedure to be investigated as a candidate for solar cell applications.[35] While Yamamoto polymerizations require elevated temperatures and air-free environments, in this case oxidative polymerization at ambient proved effective as well.

3.2. Polymer Characterization. The structures of the repeat units of **P1**−**P3** are supported by ^{1}H NMR and matrix-assisted laser desorption/ionization mass spectrometry (MALDI-MS) (see the Experimental Section). The MALDI-MS of **P2** and **P3** are shown in Figure 2 (the MALDI-MS of **P1** was reported in previous work from our group[53]). Using trans-2-[3-(4-*tert*-butylphenyl)-2-methyl-2-propenylidene]malononitrile (DCTB)[54] as the matrix, ions up to nearly m/z 15,000 and 16,000 were respectively detected for **P2** and **P3** (up to about m/z 9000 in the case of **P1**), hence supporting the presence of higher molecular weight fractions. As illustrated in Figure 2a, the mass spectrum of **P2** has ion series (n = 2−13) with spacings of ca. 1097 amu between ions, which is in good agreement with the calculated mass of the repeat unit (1095.6 amu). Similarly, the mass spectrum of **P3** presented as Figure 2b indicates that the separation between peaks (976 amu) is consistent with the polymer repeat unit (975.5 amu). Here, while oligomers consisting of 2−16 repeat units are detected, tetrameric and octameric oligomer ions dominate the spectrum. The masses of ions throughout this oligomer series is consistent with H/H end groups (as determined from the residual masses).

The ion series for polymers detected by MALDI-MS generally occur at lower masses than those estimated by

(47) Prosa, T. J.; Winokur, M. J.; Moulton, J.; Smith, P.; Heeger, A. J. *Macromolecules* **1992**, *25*, 4364.
(48) Yap, B. K.; Xia, R.; Campoy-Quiles, M.; Stavrinou, P. N.; Bradley, D. D. C. *Nat. Mater.* **2008**, *7*, 376.
(49) Stille, J. K. *Angew. Chem., Int. Ed.* **1986**, *25*, 508.
(50) Osaka, I.; McCullough, R. D. *Acc. Chem. Res.* **2008**, *41*, 1202.
(51) Lu, G.; Usta, H.; Risko, C.; Wang, L.; Facchetti, A.; Ratner, M. A.; Marks, T. J. *J. Am. Chem. Soc.* **2008**, *130*, 7670.
(52) Usta, H.; Lu, G.; Facchetti, A.; Marks, T. J. *J. Am. Chem. Soc.* **2006**, *128*, 9034.
(53) Beaujuge, P. M.; Vasilyeva, S.; Ellinger, S.; McCarley, T. D.; Reynolds, J. R. *Macromolecules* **2009**, *42*, 3694–3706.
(54) Wyatt, M. F.; Stein, B. K.; Brenton, A. G. *Anal. Chem.* **2006**, *78*, 199.

Table 1. GPC Estimated Molecular Weights of the Copolymers P1, P2, and P3 (from THF) and their Local Absorption Maxima (Solution and Solid State)

					λ_{abs} (nm) in toluene		λ_{abs} (nm) thin film		
polymer	M_n (g mol^{-1})	PDI	av no. of repeat units	av no. of rings	**1**	**2**	**1**	**2**	T_d (°C)[b]
P1	16,300	2.6	20	60	391	638	399	653 (708)[a]	321
P2	43,000	2.1	39	195	430	613	446	651	322
P3	69,300	1.6	71	355	422	591	448	636	321

[a] Shoulder. [b] Onset decomposition temperature measured by TGA under nitrogen.

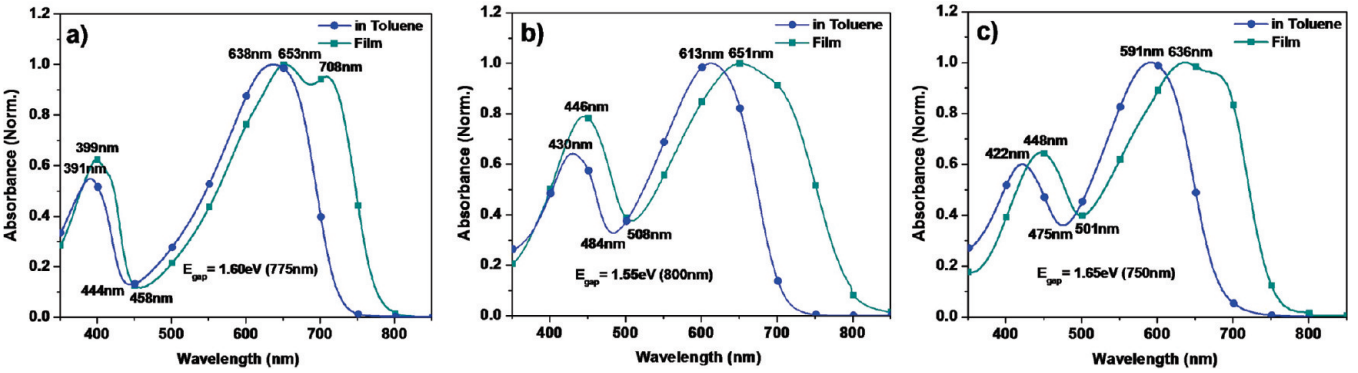

Figure 3. Solution (in toluene) and thin film optical absorption spectra of DA-copolymers **a**) **P1**, **b**) **P2**, and **c**) **P3**. The spectra of each system are normalized at the longer wavelength absorption maximum. (Figure 3c was adapted with permission from *ACS Appl. Mater. Interfaces* **2009**, *1*, 1154−1158. Copyright 2009 American Chemical Society).

gel permeation chromatography (GPC), which can essentially be explained by the discrimination of the higher mass ions taking place both during ionization and detection (phenomenon amplified with increasing polymer polydispersity).[55−57] The GPC-estimated number average molecular weights shown in Table 1 (polystyrene-calibration) range from 16,300 (for **P1**) to 69,300 g mol^{-1} (for **P3**), with relatively narrow PDIs (1.6−2.6). It is worth noting that these values were obtained without fractionating the corresponding polymers with various solvents of increasing polarity and boiling point, hence demonstrating the relevance of our chosen synthetic route involving long oligomers with low oxidation potentials as the precursors for polymerization to provide bulk amounts of polymer. Importantly, all polymers had a minimum average number of repeat units of 20 (**P1**) resulting in a backbone of about 60 aromatic units. It is generally accepted that this is ca. four times the value required to saturate the electronic properties of donor−acceptor conjugated polymers (~15 aromatic rings).[41]

Thermogravimetric analysis of **P1**, **P2**, and **P3** revealed only negligible weight loss below ~320 °C (under nitrogen), demonstrating their excellent thermal stability.

3.3. Polymer Optical Absorption. Figure 3 and Table 1 overview the optical absorption features for the polymers in toluene and as cast thin films. While all the copolymers exhibit a two-band absorption in the UV−visible, their short-wavelength optical transitions differ in terms of relative intensity and position with respect to their longer wavelength transitions. In solution, **P1** has its first local maximum of absorption in the UV (391 nm) and at a distance of ~250 nm from the second one (638 nm). In the case of **P2** and **P3**, the first local maxima are in the visible (430 and 422 nm, respectively) and separated by less than 190 nm from the second, thereby inducing a significant overlap between short and long wavelength optical transitions and shifting the window of transmission toward the higher wavelengths. In the solid state, the corresponding windows of transmission are further shifted toward the green region of the visible spectrum (480−550 nm), which provides **P2** and **P3** with a green hue in their neutral state. In contrast, the shorter wavelength optical transition of **P1** remains comparatively less intense and less shifted than that of **P2** and **P3**. As a result, **P1** shows a saturated blue hue in its neutral state.

While we attribute the lower energy transition to the intramolecular donor−acceptor interaction arising from the bonding of electron rich (DOTs) and electron deficient (BTDs) building units, the higher energy transition can be assigned to the electron-donating contribution of the alternating polymer backbone as described in previous work from our group.[38]

3.4. Polymer Electrochemistry. The redox properties of **P1**, **P2**, and **P3** were investigated via cyclic voltammetry (CV) and differential pulse voltammetry (DPV) in order to determine how polymer oxidation/reduction potentials, corresponding HOMO/LUMO energy levels and electrochemical bandgaps vary with the presence and nature of the conjugated spacer. These results are illustrated in Figure 4 and summarized in Table 2 along with the polymer optical bandgaps as determined from the onset of their lower energy transition (thin-film value). Polymer thin films were drop-cast onto platinum disk

(55) Montaudo, G.; Montaudo, M. S.; Puglisi, C.; Samperi, F. *Rapid Commun. Mass Spec* **1995**, *9*, 453.
(56) Schriemer, D. C.; Li, L. *Anal. Chem.* **1997**, *69*, 4176.
(57) Axelsson, J.; Scrivener, E.; Haddleton, D. M.; Derrick, P. J. *Macromolecules* **1996**, *29*, 8875.

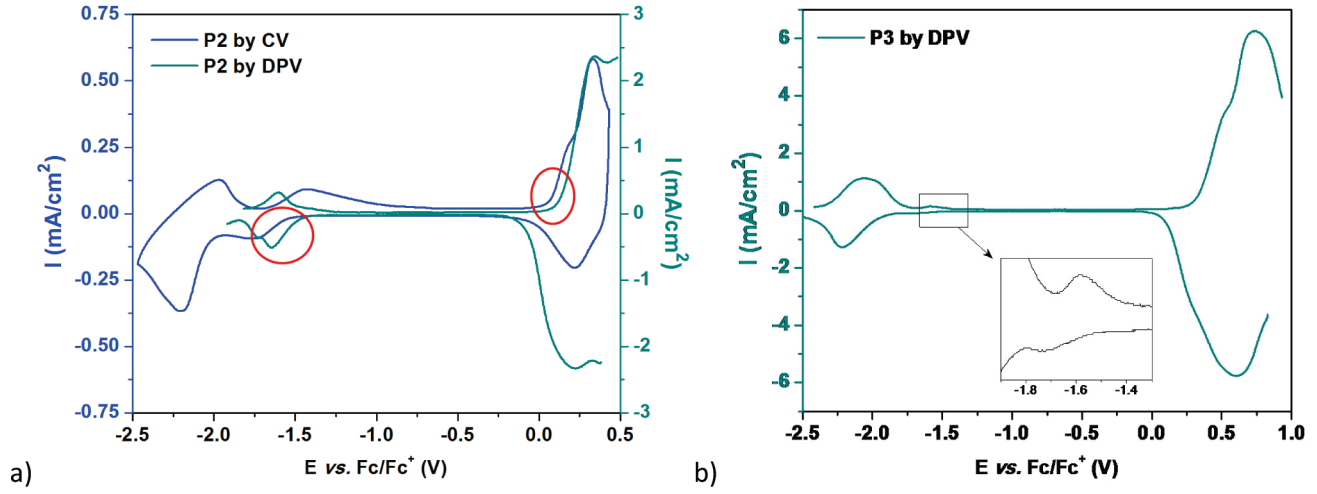

Figure 4. **a**) Cyclic (scan rate of 50 mV/s) and differential pulse voltammograms (step time of 0.1 s) of **P2** drop-cast onto a platinum disk electrode (0.02 cm^2) in 0.1 M TBAP/PC electrolyte solution and **b**) differential pulse voltammogram of **P3** (same conditions). (Figure 4b was adapted with permission from *ACS Appl. Mater. Interfaces* **2009**, *1*, 1154−1158. Copyright 2009 American Chemical Society).

Table 2. Electrochemically Determined HOMO and LUMO Levels, Electrochemical Bandgaps, and Comparison with their Optically Estimated Values for the Copolymers P1, P2, and P3[a]

	$E_{ox}onset$ (V)		HOMO (eV)		$E_{red}onset$ (V)		LUMO (eV)		E_{gap} (V)		E_{gap} (V)
polymer	CV	DPV	CV	DPV	CV	DPV	CV	DPV	CV	DPV	optical
P1	0.25	0.25	5.35	5.35	−1.57	−1.52	3.53	3.59	1.82	1.77	1.6
P2	0.18	0.14	5.28	5.24	−1.63	−1.48	3.47	3.62	1.81	1.62	1.55
P3	0.50	0.43	5.60	5.53	−1.60	−1.47	3.50	3.63	2.1	1.9	1.65

[a] Oxidation ($E_{ox}onset$) and reduction ($E_{red}onset$) potentials are reported vs Fc/Fc^+. HOMO and LUMO energy levels are derived from the electrochemical data ($E_{ox}onset$ and $E_{red}onset$, respectively) considering that the SCE is 4.7 eV vs vacuum[58] and Fc/Fc^+ is 0.38 eV vs SCE,[59] i.e. 5.1 eV relative to vacuum.

electrodes from toluene solutions (6 mg mL^{-1}) and characterized in an argon-filled drybox using a platinum flag as the counter electrode and a silver wire as the reference electrode. The estimated potentials were subsequently calibrated to Fc/Fc^+. The corresponding polymer energy levels are reported relative to the vacuum level, considering that the SCE is 4.7 eV vs vacuum[58] and Fc/Fc^+ is 0.38 eV vs SCE,[59] i.e. ∼5.1 eV relative to vacuum. The polymer films were cycled until they reached a stable and reproducible redox response prior to characterization.

We have previously described the redox characteristics of **P1**. In brief, a low oxidation potential of +0.25 V corresponding to a relatively high HOMO energy level of 5.35 eV relative to vacuum was found via CV and supported by DPV. The onset of reduction was found at −1.57 V by CV and −1.52 V by DPV, corresponding to a LUMO of 3.53 and 3.59 eV, respectively. These results yield electrochemical bandgaps of 1.82 and 1.77 eV depending on the method employed.

The CV and DPV traces of **P2** are illustrated in Figure 4a. As expected, **P2** revealed a lower oxidation potential than that of **P1**, +0.18 V by CV and +0.14 V by DPV, and a higher HOMO, 5.28 eV from CV and 5.24 eV from DPV, owing to the incorporation of the electron-rich bi-3,4-dimethoxythiophene conjugated spacer. The signal corresponding to the first reduction process observed was weaker than that of the second reduction seen by CV, the later one (reduction of the electron-rich segments) inducing degradation of the polymer on repeated cycling. The onset of reduction estimated from the first reductive process, −1.63 V by CV and −1.48 V by DPV, is consistent with the literature for BTD-containing DA copolymers.[13,16,53,60] From the corresponding LUMOs, 3.47 eV by CV and 3.62 eV by DPV, energy gaps of 1.81 and 1.62 eV are estimated by each method, respectively, in agreement with those found for **P1**.

We have recently reported on the redox characteristics of **P3**.[61] In contrast with **P2**, the introduction of a bithienyl conjugated spacer in **P3** repressed the polymer HOMO (5.60 eV by CV and 5.53 eV by DPV). This is explained by the less pronounced electron-rich character of thiophene when compared to that of dimethoxythiophene. Hence, polymer **P3** exhibits a higher oxidation potential (+0.50 V by CV and +0.43 V by DPV) than **P1** and **P2** while retaining a similar onset of reduction (−1.6 V by CV and −1.47 V by DPV). In analogy with **P2**, the signal associated with the first reduction process is much less intense than that of the second reduction (see Figure 4b) which induced degradation of the polymer on repeated cycling.

(58) Hansen, W. N.; Hansen, G. J. *Phys. Rev. A* **1987**, *36*, 1396.
(59) Pavlishchuk, V. V.; Addison, A. W. *Inorg. Chem. Acta* **2000**, *298*, 97.
(60) Blouin, N.; Michaud, A.; Leclerc, M. *Adv. Mater.* **2007**, *19*, 2295.
(61) Subbiah, J.; Beaujuge, P. M.; Choudhury, K. R.; Ellinger, S.; Reynolds, J. R.; So, F. *ACS Appl. Mater. Interfaces* **2009**, *1*, 1154–1158.

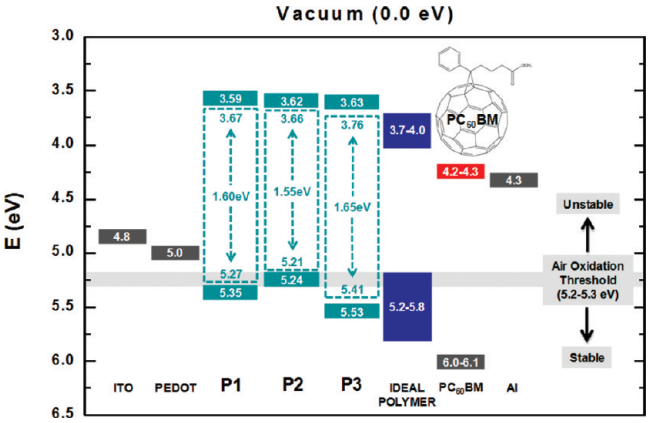

Figure 5. Energy-level diagram showing the HOMO and LUMO energies of **P1**−**P3** as estimated by DPV (green filled rectangles) relative to those of an "ideal polymer" (designed for use with $PC_{60}BM$ and PEDOT-PSS in BHJ solar cells). The respective optically determined bandgaps were placed at the baricenter of the electrochemical bandgaps, and a second approximated set of HOMO and LUMO levels could be defined assuming the energy levels equidistant from the baricenter (in the green dotted rectangle).

In general, the DPV estimated bandgaps were found to be slightly smaller (by up to 0.2 eV) than those determined by CV. In fact, as DPV minimizes the contribution of the charging background currents, it commonly provides higher sensitivity and sharper redox onsets than CV when investigating π-conjugated polymers.[53,62] Further, all electrochemical bandgaps were found to be slightly larger than the optically estimated values as reported in work on DA polymers from various groups[7,41,63] but remain in good agreement. For example, the CV determined bandgap of **P2** (1.81 eV) differs from its optically estimated gap (1.55 eV) by 0.26 eV, but the gap obtained by DPV (1.62 eV) only differs by ca. 0.1 eV. In parallel, the CV determined bandgap of **P3** (2.1 eV) differs significantly from its optically estimated gap (1.55 eV), but the gap obtained by DPV (1.9 eV) only differs by 0.3 eV.

Following these considerations, the DPV estimated energy levels of the polymers were employed in the construction of the energy diagram shown as Figure 5 which correlates the band structure of the semiconducting polymers with respect to the different energy levels associated with the components commonly included in the fabrication of photovoltaic devices (ITO, PEDOT:PSS, $PC_{60}BM$, Al).[13,64] The relatively deep HOMO level of **P3** in comparison with that of **P1** and **P2** should induce a reduced reactivity to oxygen and an increased open-circuit voltage in the subsequent solar cells and should then impact their overall power conversion efficiency.[4,6]

3.5. Polymer Photovoltaic Performance. *3.5.a. Device Optimization Study*. The PV properties of **P1**−**P3** were investigated in donor−acceptor bulk heterojunction (BHJ) solar cells with $PC_{60}BM$ as the acceptor, under simulated AM 1.5 solar illumination (at an irradiation intensity of 100 mW cm^{-2}). The composition of the copolymer-PCBM blends, spin-cast from chlorobenzene in devices using PEDOT-PSS-coated ITO glass substrate, was first optimized. Figure 6 compares the current density−voltage (*J*-*V*) plots for devices with **P1** (blue curve), **P2** (green curve), and **P3** (red curve) at optimized polymer:PCBM composition.

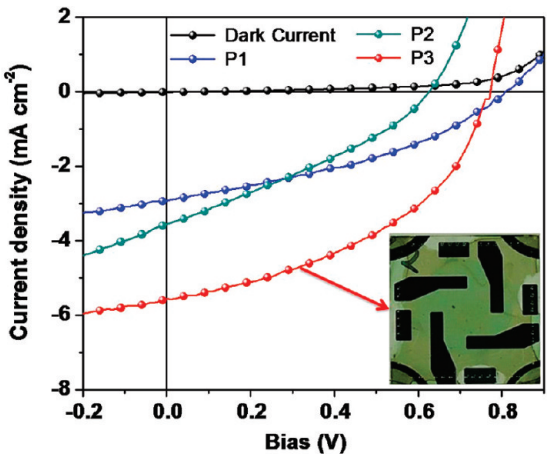

Figure 6. *I*−*V* curves of **P1**−**P3**-based PSCs (at best polymer:PCBM composition) under AM 1.5 solar illumination, 100 mW cm^{-2}. The photograph illustrates the green hue attained in the case of **P3** at the polymer:PCBM ratio of 1:8 (the device is backlit such that the Al contacts appear black). Devices with post-polymer processing thermal treatment at 70 °C (30 min). The device structure is ITO/PEDOT/PX:$PC_{60}BM$/LiF/Al with PX = **P1**, **P2**, or **P3**.

Table 3. Solar Cell Device Performance for P1-Based PSCs[a] as a Function of Polymer:PCBM Blend Composition[b]

P1:$PC_{60}BM$ (w/w)	J_{sc} (mA cm^{-2})	V_{oc} (V)	FF (%)	PCE (%)
1:4	**2.92**	**0.80**	**38**	**0.88**
1:6	2.15	0.80	42	0.73

[a] Under AM 1.5 illumination at an irradiation intensity of 100 mW cm^{-2}. [b] Devices with post-polymer processing thermal treatment at 70 °C (30 min). The device structure is ITO/PEDOT/P1:$PC_{60}BM$/LiF/Al.

Table 4. Solar Cell Device Performance for P2-Based PSCs[a] as a Function of Polymer:PCBM Blend Composition[b]

P2:$PC_{60}BM$ (w/w)	J_{sc} (mA cm^{-2})	V_{oc} (V)	FF (%)	PCE (%)
1:4	1.90	0.58	33	0.37
1:5	**3.56**	**0.62**	**32**	**0.70**
1:6	3.08	0.58	33	0.58
1:8	2.60	0.58	36	0.54

[a] Under AM 1.5 illumination at an irradiation intensity of 100 mW cm^{-2}. [b] Devices with post-polymer processing thermal treatment at 70 °C (30 min). The device structure is ITO/PEDOT/P2:$PC_{60}BM$/LiF/Al.

The PV results for the device using the neutral state blue copolymer **P1** are summarized in Table 3. In reproducing the experiments carried out by Janssen et al. for comparison,[35] a device was made with a polymer:PCBM ratio of 1:4 (by weight), revealing near-identical PV characteristics. In our laboratories, the **P1**-based device showed a short-circuit current density (J_{SC}) of 2.92 mA cm^{-2}, an open-circuit voltage (V_{OC}) of 0.80 V, and a fill factor (FF) of 38%. The resulting overall power conversion efficiency (PCE) was found to reach 0.8% which is in good agreement with the PCE of 0.9% reported by Janssen et al. It is

(62) DuBois, C. J.; Abboud, K. A.; Reynolds, J. R. *J. Phys. Chem. B* **2004**, *108*, 8550.
(63) Hou, J.; Tan, Z.; Yan, Y.; He, Y.; Yang, C.; Li, Y. *J. Am. Chem. Soc.* **2006**, *128*, 4911.
(64) Li, G.; Shrotriya, V.; Huang, J. S.; Yao, Y.; Moriarty, T.; Emery, K.; Yang, Y. *Nat. Mater.* **2005**, *4*, 864.

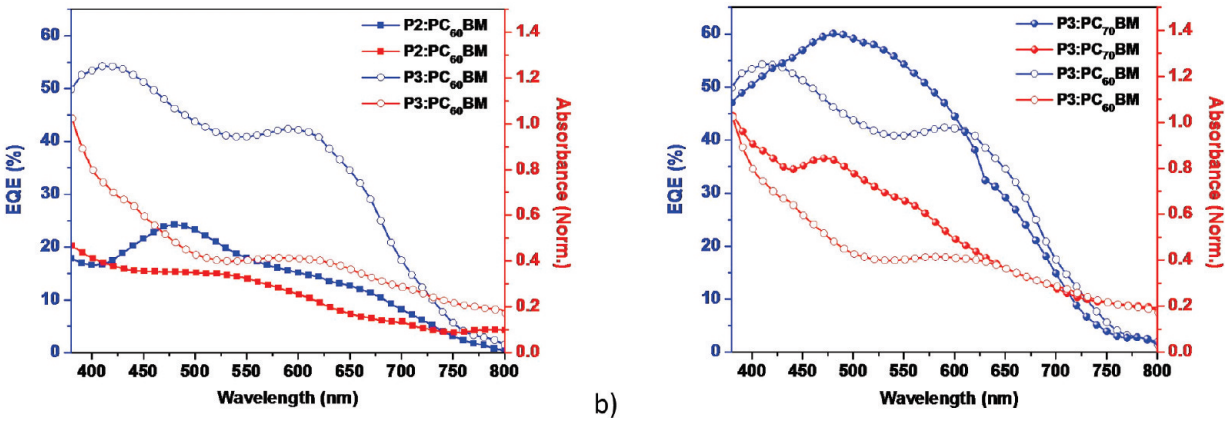

Figure 7. **a**) Superimposed EQE (blue curves) and polymer:PCBM blend absoprtion (red curves) for **P2** (filled squares) and **P3** (empty circles)-based PSCs (at optimized polymer:PCBM composition) and **b**) superimposed EQE (blue curves) and polymer:PCBM blend absoprtion (red curves) for **P3**-based PSCs (at best polymer:PCBM composition) with the configuration ITO/PEDOT/**P3**:$PC_{60}BM$/LiF/Al (empty circles) and ITO/MoO_3/**P3**:$PC_{70}BM$/LiF/Al (filled circles).

important to note that, although **P1** was prepared and purified using different methods in our work relative to that of the Janssen group, the agreement between our results demonstrates the quality of our polymer which was synthesized under oxidative polymerization conditions (as opposed to a Ni-catalyzed Yamamoto-type polycondensation) and subsequently reduced with hydrazine. Overall, in spite of its high V_{OC}, the performance of the low-bandgap polymer **P1** remains limited at the best polymer:PCBM blend composition, which could be due to the poor charge-transport in the photoactive layer, an unfavorable blend morphology (poor interpenetrating network, pronounced phase segregation), or the combination of both. The importance of the polymer charge-carrier mobility in PV devices has recently been described by Li et al. and other groups.[4,19,65,66]

Considering electron−hole recombinations as being a primary limiting-factor in the performance of PV devices made with relatively low-mobility semiconducting polymers,[4,66] we have investigated ways to planarize the backbone of **P1** via the use of bithienyl spacers substituted with short (**P2**) or with no (**P3**) side groups. In a similar approach, Marks et al. have clearly demonstrated the influence of unsubstituted bithienyl spacers on the hole mobility of all-donor semiconducting polymers.[52,67]

The PV results for devices using the neutral state green copolymer **P2** comprising a bi-(3,4-dimethoxythienylene) spacer are summarized in Table 4. These substituents were chosen to provide an electron rich linker which would have only a minimal amount of steric interaction disrupting the planarity of the linking unit. Optimization of the polymer:PCBM composition showed that the best device performance was obtained at a ratio of 1:5 (by weight, i.e. 83.3% in PCBM content), and a further increase of the PCBM content did not enhance the PV response. This optimized **P2**-based device showed a higher J_{SC} of 3.56 mA cm^{-2} but a notably lower V_{OC} of 0.62 V and a lower FF of 32% when compared to the best device made with **P1** (FF = 38%). The lower V_{OC} of **P2** coincides with the high-lying HOMO level, estimated electrochemically to be 5.24 eV relative to vacuum by DPV. The resulting PCE was 0.70% under AM 1.5, thereby lower than that observed for the best **P1**-based PV device. Surprisingly, in spite of its broad two-band absorption over the visible and reduced concentration in solubilizing groups along the backbone, **P2** did not provide any improvement over **P1**. This is confirmed by the relatively low external quantum efficiency (EQE) of ca. 24% obtained at 480 nm (see Figure 7a). Here again, the performance limitation could stem from charge-recombination considerations, a poor interpenetrating network, or the combination of both.

As a result, **P3** was investigated as an alternative to **P2** in terms of the targeted color state (green). The PV results from the neutral state green copolymer **P3** composed of an unsubstituted bithiophene spacer are summarized in Table 5. PSCs fabricated with **P3** were shown to be very sensitive to the PCBM content in the blend, and at the optimum polymer:PCBM composition of 1:8, a J_{SC} as high as 5.56 mA cm^{-2}, a V_{OC} of 0.77 V near-equal to that of **P1**, and an improved FF of 44% were obtained. The resulting overall PCE was up to 1.90% under 1 Sun. The V_{OC} of **P3**, similar to that of **P1**, is in excellent agreement with the electrochemically obtained deep HOMO value of 5.53 eV (relative to vacuum, by DPV). The EQE data of **P3** are compared to that of **P2** in Figure 7a. A two-band response is observed with the long wavelength maximum attributed to the long wavelength absorption band of the polymer. The short wavelength maximum is due to the absorption by PCBM combined with that of the short wavelength absorption band of the polymer. The onset of photocurrent at 750 nm is in agreement with the optical absorption results (overlaid in Figure 7a). It is worth noting that the EQE of the device with **P3** having 80% PCBM (blend ratio of 1:4) showed a maximum of 28% at 460 nm, whereas that of the device with 88.9% PCBM (blend ratio of 1:8) showed a maximum of 54% at the

(65) Mandoc, M. M.; Koster, L. J. A.; Blom, P. W. M. *Appl. Phys. Lett.* **2007**, *90*, 133504.
(66) Koster, L. J. A.; Mihailetchi, V. D.; Blom, P. W. M. *Appl. Phys. Lett.* **2006**, *88*, 093511.
(67) Lu, G.; Usta, H.; Risko, C.; Wang, L.; Facchetti, A.; Ratner, M. A.; Marks, T. J. *J. Am. Chem. Soc.* **2008**, *130*, 7670.

Table 5. Solar Cell Device Performance for P3-Based PSCs[a] as a Function of Polymer:$PC_{60}BM$ Blend Composition[b]

P3:$PC_{60}BM$ (w/w)	J_{sc} (mA cm^{-2})	V_{oc} (V)	FF (%)	PCE (%)
1:4	1.99	0.78	41	0.64
1:6	3.93	0.77	46	1.39
1:7	4.79	0.76	46	1.68
1:8	**5.56**	**0.77**	**44**	**1.90**
1:9	3.97	0.73	35	1.00
1:10	2.10	0.71	40	0.60

[a] Under AM 1.5 illumination at an irradiation intensity of 100 mW cm^{-2}. [b] Devices with post-polymer processing thermal treatment at 70 °C (30 min). The device structure is ITO/PEDOT/**P3**:$PC_{60}BM$/LiF/Al.

same wavelength, thereby supporting the device sensitivity to the proportion of PCBM used in the blend observed throughout the polymer:PCBM optimization study. When we studied the optical absorption of the PSC at the blend ratios 1:4, 1:6, and 1:8, we found that there was no substantial difference between the absorption spectra of all the blends, and we attributed the notable enhancement in EQE in the case of **P3** to an increase in charge-carrier mobility, similar to that observed in the MDMO-PPV:PCBM systems.[61]

With the goal of probing the effect of a significant increase of PCBM on the PV properties of **P1**, a device was made with a polymer:$PC_{60}BM$ ratio of 1:6 (see Table 3). In contrast to the results obtained for **P3**, the increase of fullerene in the blend (from 80% to 85.7%) did not improve the PCE (0.73%). In this case, the J_{SC} decreased to an average of 2.15 mA cm^{-2}, hence confirming that the blend composition initially suggested by Janssen et al. provides the optimum PV performance of **P1**.

In addition to the determining role of the donor−acceptor blend composition on the PV device performance, the nature of the interface material employed between the metal oxide electrode and the organic active layer influences the hole extraction efficiency. Several groups have recently demonstrated that metal oxides such as NiO_X, MoO_3, and V_2O_5 can considerably enhance the performance of polymer solar cells by replacing PEDOT-PSS as the hole-transporting interface layer.[68,69] Here, we have investigated the performance of vapor deposited MoO_3 as an interface layer between ITO and the polymer:$PC_{60}BM$ active layer in devices made with **P3** (see Table 6). When PEDOT was replaced by MoO_3 (~10 nm) in a device using the best polymer:$PC_{60}BM$ blend composition, the FF increased from 46% to 51%, and, in turn, the device PCE was raised from 1.90% to 2.12%. Increases in FF can generally be explained by a diminution of the concentration of electron−hole recombinations across the active layer.[4] Considering that MoO_3 is an n-type semiconductor with an electron affinity of ~5.8 eV (relative to vacuum),[69−71] the alignment between the HOMO level of **P3** and the conduction band-edge of MoO_3 leads to enhanced hole extraction and reduction in contact resistance. In this device architecture, J_{SC} (5.38 mA cm^{-2}) and V_{OC} (0.77 V) remain near-identical to the values obtained for the PEDOT-based device configuration.

Table 6. Optimization of the Solar Cell Device Performance for P3[a] by Varying the Hole-Transporting Interface Layer (PEDOT or MoO_3) and the Type of PCBM Used ($PC_{60}BM$ or $PC_{70}BM$)[b]

P3	J_{sc} (mA cm^{-2})	V_{oc} (V)	FF (%)	PCE (%)
MoO_3/$PC_{60}BM$	5.38	0.77	51	2.12
PEDOT/$PC_{70}BM$	5.90	0.80	48	2.31
MoO_3/$PC_{70}BM$	**5.96**	**0.80**	**57**	**2.71**

[a] Under AM 1.5 illumination at an irradiation intensity 100 mW cm^{-2}. [b] Devices with postfabrication thermal treatment at 70 °C (30 min).

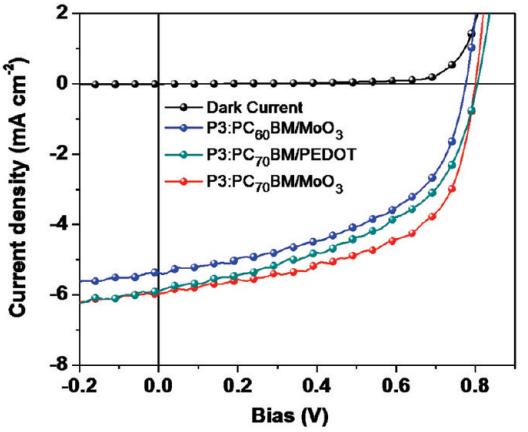

Figure 8. *I*−*V* curves of **P3**-based PSCs (at best polymer:PCBM composition, i.e 1:8) in the dark (black curve) and under AM 1.5 solar illumination, 100 mW cm^{-2}, for various device configurations. The device structures are ITO/MoO_3/**P3**:$PC_{60}BM$/LiF/Al (blue curve), ITO/PEDOT/**P3**:$PC_{70}BM$/LiF/Al (green curve), and ITO/MoO_3/**P3**:$PC_{70}BM$/LiF/Al (red curve). Devices with post-polymer processing thermal treatment at 70 °C (30 min).

Finally, as illustrated in Figure 8 and Table 6 we have investigated the use of $PC_{70}BM$ as an acceptor in combination with PEDOT-PSS or MoO_3 as the hole-extracting interface layer in the best composition **P3**-based cell. With its visible absorption (higher-lying HOMO than $PC_{60}BM$ which absorbs essentially in the UV), $PC_{70}BM$ has commonly led to performance enhancements in BHJ donor−acceptor PV devices employing semiconducting polymers as the electron-donating component.[7,12] For the P3:$PC_{70}BM$ cells with PEDOT-PSS as the hole transporting interface layer, the J_{SC} increased to an average of 5.90 mA cm^{-2}, and the V_{OC} increased slightly to 0.80 V, possibly due to a difference in blend morphology. In addition, there is also an increase of FF (48%), and the resulting PCE was raised to 2.31%. When MoO_3 was used as the hole-extracting interface layer, the J_{SC} increased again to an average of 5.96 mA cm^{-2}, and the V_{OC} remained the same (0.80 V). More importantly, the corresponding FF increased from 48% to 57%, which significantly enhanced the overall PCE to 2.71%. The EQE results for **P3:**$PC_{70}BM$ are compared to those of **P3:**

(68) Irwin, M. D.; Buchholz, D. B.; Hains, A. W.; Chang, R. P. H.; Marks, T. J. *Proc. Natl. Acad. Sci. U.S.A.* **2008**, *105*, 2783.
(69) Vishal, S.; Gang, L.; Yan, Y.; Chih-Wei, C.; Yang, Y. *Appl. Phys. Lett.* **2006**, *88*, 073508.
(70) Kröger, M.; Hamwi, S.; Meyer, J.; Riedl, T.; Kowalsky, W.; Kahn, A. *Org. Electron.s* **2009**, *10*, 932.
(71) Kim, D. Y.; Subbiah, J.; Sarasqueta, G.; So, F.; Ding, H.; Irfan, Gao, Y. *Appl. Phys. Lett.* **2009**, *95*, 093304.

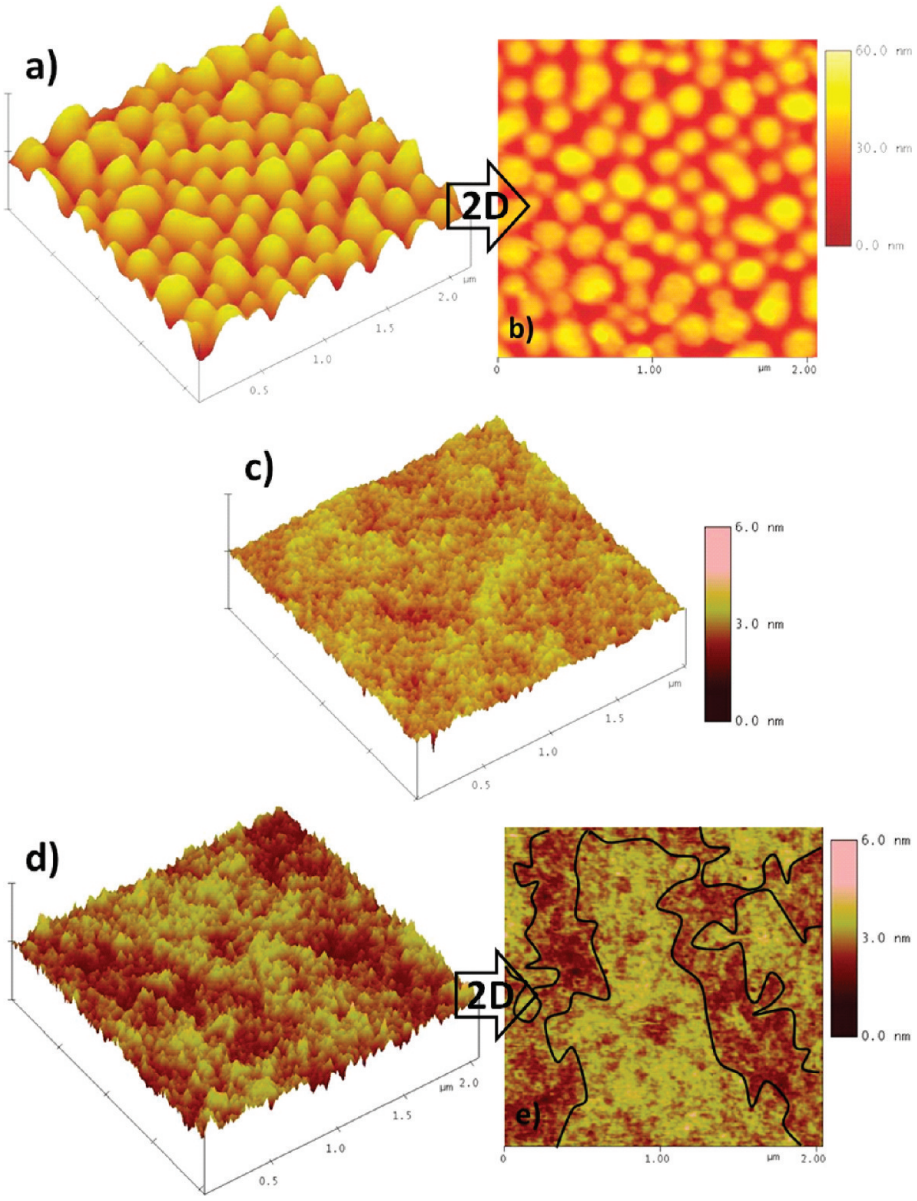

Figure 9. AFM tapping-mode images of **P1**−**P3** in blend with $PC_{60}BM$ (best compositions are represented). Film surfaces from devices with post-polymer processing thermal treatment at 70 °C (30 min). **a**) and **b**) P1:$PC_{60}BM$, **c**) P2:$PC_{60}BM$, and **d**) and **e**) P3:$PC_{60}BM$. All images are 2 × 2 μm.

$PC_{60}BM$ in Figure 7b. This time, a broadband response was observed, peaking at ~60% at 480 nm as the optical absorption spectrum of $PC_{70}BM$ complements that of copolymer **P3** in the 410−620 nm range (the device took a brown-red hue). The onset of the photocurrent at 750 nm was also in agreement with the blend optical absorption (overlaid in Figure 7b). Here, the notable enhancement in EQE is likely due to an improved spectral absorption in the visible. In addition, we do not exclude the possibility of a combined increase in charge-carrier mobility for the blend when $PC_{70}BM$ is used, and work investigating this possibility is currently underway.

3.5.b. Morphology Study. In an effort to understand how the blend morphology evolves as a function of the copolymer employed as the electron-rich component in the donor−acceptor BHJ, the active layer of the PV devices at their optimized polymer:PCBM composition was investigated by atomic force microscopy (AFM) in the tapping-mode using actual devices, and imaging regions where the top contacts were not present. In each case, a thermal treatment step (70 °C, 30 min) was carried out prior to Al contacts deposition.

Figure 9a,b illustrates the 3D- and 2D-images, respectively, of the **P1**-based PV device surface. From these AFM images, a particularly coarse morphology is observed which points toward a relatively pronounced phase segregation (demixing) between PCBM and the polymer, as previously proposed.[32,72,73] In this case, an interpenetrating network is not evident, which is consistent with the limited performance of the devices with

(72) Lee, J. K.; Ma, W. L.; Brabec, C. J.; Yuen, J.; Moon, J. S.; Kim, J. Y.; Lee, K.; Bazan, G. C.; Heeger, A. J. *J. Am. Chem. Soc.* **2008**, *130*, 3619.
(73) Wienk, M. M.; Kroon, J. M.; Verhees, W. J. H.; Knol, J.; Hummelen, J. C.; Hal, P. A. v.; Janssen, R. A. J. *Angew. Chem., Int. Ed.* **2003**, *42*, 3371.

P1 as the semiconducting material. The distinct domains of higher heights (up to 60 nm, rms roughness = 7.561 nm) are attributed to the formation of PCBM clusters, similar to what has been observed by other groups.[74,75] Figure 9c shows the 3D-image of the **P2**-based PV device surface. From this image, a much more homogeneous morphology is observed with heights limited to 0.386 nm of rms roughness, suggesting a minimal extent of phase separation in the blend. A certain extent of phase separation between donor and acceptor in the BHJ remains a necessary condition in the formation of the bicontinuous network desired to attain efficient PV devices.[72] In contrast, the 3D- and 2D-images of the **P3**-based PV device surface shown in Figures 9d and 9e display a more heterogeneous morphology where relatively large domains of higher heights are dispersed within the active layer. These domains have been outlined in black in the 2D-view of the corresponding AFM image. Considering the high PCBM content (~88.9%) of the **P3**-based device at best composition (1:8 by weight, polymer to PCBM), it is reasonable to assign these domains to a PCBM-rich phase, with no indication of "overgrown" PCBM-cluster formation.

With these distinctly different morphologies expressed in the blends, we further investigated the charge-transport properties of the active layer composing our devices. The results would yield additional information on the differences observed in the PV properties of **P1**−**P3** in BHJs with PCBM.

3.5.c. Current−*Voltage Measurements.* The photocurrent in donor−acceptor organic PV cells is governed not only by the free electron−hole pair generation rate but also by recombination processes which depend on the mean free path of carriers.[76] This, in turn, depends on the charge-carrier mobility and the carrier lifetime.[77] Hence, the charge-transport properties of the semiconductor can have a strong impact on the photoresponse of the cells. For polymers with low carrier mobility, the charge transport in BHJ photovoltaic cells is expected to be significantly imbalanced due to the difference in electron and hole mobilities, leading to charge build-up and increased recombination processes. In order to understand the variations in performance of the three copolymers (**P1**−**P3**) used here, we studied the charge-carrier transport in the pristine polymer and compared it to results from polymer:PCBM blends with optimized compositions for photovoltaic performance.

We have previously observed the dark current in pristine copolymer **P3** to be space-charge limited (SCL),[61] allowing for the direct determination of hole mobility from simple current density−voltage (*J*-*V*) measurements. This method is frequently used to determine the carrier mobility in low mobility media. From the *J*-*V* data, the hole mobility can be estimated using the Mott-Gurney equation for trap-free SCL current

$$J = \frac{9}{8}\mu\varepsilon\frac{V^2}{d^3}$$

where ε is the dielectric constant, μ is the charge-carrier mobility, and d is the sample thickness.

The structures of the hole-only devices studied were ITO/PEDOT-PSS/polymer or polymer:PCBM/Pd. Offering a larger barrier to electron injection into PCBM compared to the more widely used Au as electrode material, Pd was chosen as the electron-blocking counter electrode. The films were annealed at 70 °C for 30 min prior to Pd deposition. Consequently, we can treat the devices as hole-only in this analysis.

Figure 10 shows the experimental dark current densities in the hole-only devices of the three copolymers

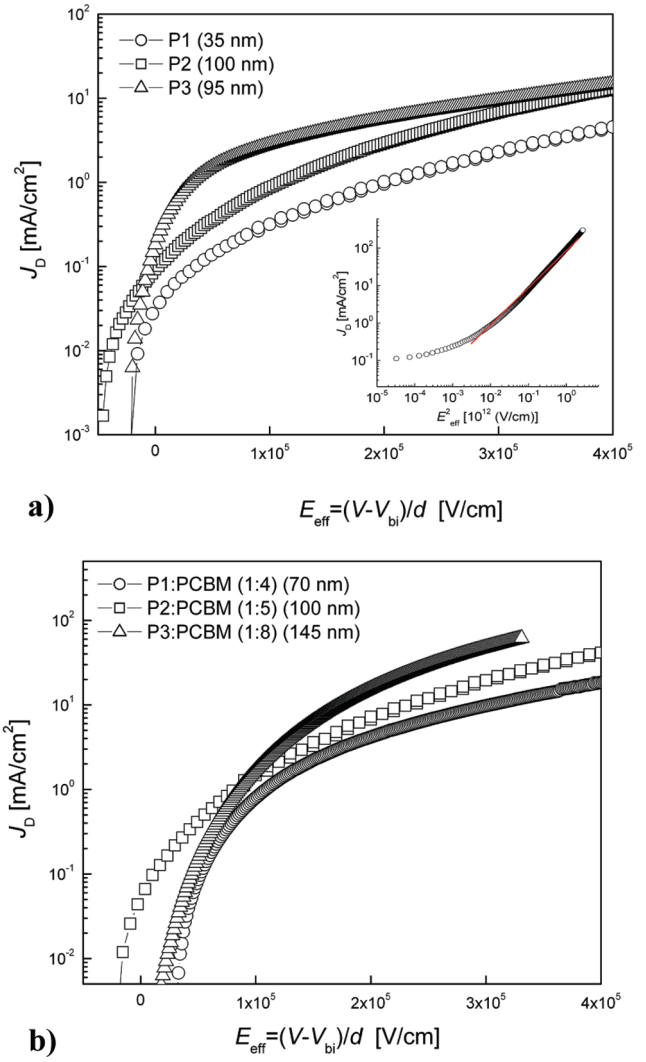

Figure 10. **a**) Experimental dark current densities for hole-only devices of copolymers **P1**, **P2**, and **P3** as a function of the effective electric field. The inset shows the quadratic dependence of dark current density on applied bias; the line is a fit using single-carrier SCLC model. **b**) *J*-*V* characteristics of hole-only polymer:PCBM blend devices with composition optimized for photovoltaic response. The legends show respective device thicknesses.

(74) Martens, T.; D'Haen, J.; Munters, T.; Beelen, Z.; Goris, L.; Manca, J.; D'Olieslaeger, M.; Vanderzande, D.; De Schepper, L.; Andriessen, R. *Synth. Met.* **2003**, *138*, 243.
(75) Hoppe, H.; Niggemann, M.; Winder, C.; Kraut, J.; Hiesgen, R.; Hinsch, A.; Meissner, D.; Sariciftci, N. S. *Adv. Funct. Mater.* **2004**, *14*, 1005.
(76) Alvin, M. G.; Albert, R. *J. Appl. Phys.* **1971**, *42*, 2823.
(77) Melzer, C.; Koop, E. J.; Mihailetchi, V. D.; Blom, P. W. M. *Adv. Funct. Mater.* **2004**, *14*, 865.

Table 7. Zero-Field Hole Mobility in the Pristine Copolymers and in the Polymer Phase of the Optimized Blends, Derived from Fitting the J-V Data to the Trap-Free Single-Carrier SCLC Model

device composition	P1	P1:$PC_{60}BM$	P2	P2:$PC_{60}BM$	P3	P3:$PC_{60}BM$
zero-field hole mobility ($cm^2\ V^{-1}\ s^{-1}$)	5.4×10^{-8}	2×10^{-6}	6.9×10^{-7}	5×10^{-6}	3.9×10^{-6}	1×10^{-5}

(see Figure 10a) used in this study and of blends with PCBM loading (see Figure 10b) optimized for the best photovoltaic performance. The applied voltage V is corrected for the built-in voltage V_{bi} that results from the difference in the work function of the electrodes. To facilitate comparison of devices with different thicknesses, the current density is plotted as a function of the effective electric field, E_{eff}, rather than the applied voltage. As illustrated in Figure 10a, current densities at any electric field inside the device increase progressively from **P1** to **P2** to **P3**, especially at low device bias. The result agrees well with the expectation of increasingly higher backbone planarity in copolymers **P2** and **P3** with the diminution of the concentration of solubilizing side chains through the introduction of unsubstituted conjugated spacers. It is expected that the reduced lamellar spacing and enhanced π-stacking resulting from the incorporation of unsubstituted spacers improves charge transport in the copolymers **P2** and **P3** compared to the control **P1**. It should be noted that the current densities scaled quadratically with the applied voltage (see Figure 10a, inset), a behavior characteristic of SCLC, allowing the estimation of hole mobility in the polymers. The improved charge transport in the successive generations of copolymers is manifested clearly in Table 7, where the room temperature zero-field hole mobility increases by almost two orders in going from **P1** to **P3**.

The dark current densities of hole-only photovoltaic devices having the optimized composition (for photoresponse) of each copolymer with PCBM are presented in Figure 10b. Interestingly, the hole current in the blend devices is found to be significantly higher in all three optimized compositions compared to the devices with pristine polymers. As a consequence, the hole mobility in the donor polymer phase of the blend is also enhanced significantly, by an order of magnitude or more (see Table 7), compared to its value in the copolymers. This result may seem unexpected given the fact that the donor polymer phase is significantly diluted in the blends, which would generally lead to reduced charge transport properties due to the possibility of incomplete percolation. However, such an enhancement in hole mobility of a few PPV-based donor polymers upon blending with PCBM has been reported before,[77,78] though its origin is not very clear. It has been proposed,[77,78] that mixing with the PCBM phase leads to a favorable change in film morphology in these systems that enhances the intermolecular interaction in the donor phase, leading to improved charge transfer between polymer chains and thereby better mobility. Correlating film morphology and carrier transport, we believe that this series of dioxythiophene-benzothiadiazole donor−acceptor copolymers behave in a similar manner in blends with PCBM.

The electron mobility in the PCBM phase of a polymer:PCBM blend with high (> 70 wt %) PCBM content (as in the blend with **P3**) has previously been determined as $\sim 10^{-3}$ $cm^2\ V^{-1}\ s^{-1}$.[79] The lower-than-optimum hole mobility in our pristine green copolymers ($\sim 10^{-6}-10^{-5}$ $cm^2\ V^{-1}\ s^{-1}$) can result in unbalanced charge transport in BHJ photovoltaic cells. Blending the copolymers with an optimized large proportion of PCBM leads to a significant enhancement of hole mobility. This reduces the difference between electron and hole mobilities in the blend and improves the charge balance across the device. As a direct consequence, the photoresponse, and, in turn, the power conversion efficiency of these optimized devices, improves markedly. This observation is confirmed when copolymer **P3** is mixed with $PC_{70}BM$ in an optimized photovoltaic composition. Along with enhanced light absorption in the visible window (480−550 nm), blending with $PC_{70}BM$ also leads to an enhancement of hole mobility in the **P3** phase, which reaches a value of 9×10^{-5} $cm^2\ V^{-1}\ s^{-1}$ under short circuit condition. We attribute the 28% improvement of overall PCE in the devices employing MoO_3, for instance, to a combination of these two factors.

4. Conclusions

In summary, the structure-performance relationships in PV devices of a series of soluble donor−acceptor π-conjugated polymers comprising electron-rich 3,4-dioxythiophenes and the electron-deficient 2,1,3-benzothiadiazole (**P1**−**P3**) have been carefully investigated, with an emphasis on correlating molecular structure, energy band characteristics, and charge transport. Importantly, the synthesis and chemical polymerization of two polyheterocyclic and regiosymmetric DA oligomers (**M2** and **M3**) afforded two-band absorbing polymers reflecting/transmitting the color green (**P2** and **P3**), an important color state in the realization of power-generating displays. As the PV properties of **P1**−**P3** were investigated in DA bulk heterojunction (BHJ) devices with $PC_{60}BM$ as the acceptor, and under simulated AM 1.5 G solar illumination, it was found that the neutral state green copolymer **P3** comprising an unsubstituted bithiophene spacer exhibited a 2-fold enhancement in PCE (1.90%) over the all dioxythiophene-based copolymers **P1** and **P2** (0.88% and 0.70%, respectively). AFM-imaging of the corresponding polymer:PCBM blends (optimized composition) and careful analysis of their

(78) Mihailetchi, V. D.; Koster, L. J. A.; Blom, P. W. M.; Melzer, C.; de Boer, B.; van Duren, J. K. J.; Janssen, R. A. J. *Adv. Funct. Mater.* **2005**, *15*, 795.

(79) Mihailetchi, V. D.; Duren, J. K. J. v.; Blom, P. W. M.; Hummelen, J. C.; Janssen, R. A. J.; Kroon, J. M.; Rispens, M. T.; Verhees, W. J. H.; Wienk, M. M. *Adv. Funct. Mater.* **2003**, *13*, 43.

charge transport in hole-only devices show that there is a strong correlation between the blend morphology and the charge transport properties throughout the polymer series and support our reasoning for the synthetic design employed. Further, we have replaced PEDOT:PSS by MoO_3 and $PC_{60}BM$ by $PC_{70}BM$ in the **P3**-based devices and demonstrated a PCE of 2.71% of PCE in absence of any tedious solvent- or thermal-annealing treatment. These results confirm the importance of adjusting the device configuration as a function of the intrinsic properties (e.g., energy band structure, mobility of the charge-carriers) of the semiconducting polymers investigated. In the case of **P3**, the optical absorption of $PC_{70}BM$ complements the two-band absorption of the polymer and balances the charge transport of the blend, thereby extending the photon collection over the entire visible spectrum while raising the EQE to a maximum of ca. 60% at ~480 nm.

Beside the fine-tuning of optical absorption and charge-transport properties achieved by the simple structural modifications described in this contribution, our synthetic approach involving the chemical polymerization of regiosymmetric oligomers possessing low oxidation potentials offers the perspectives for novel and more elaborate polymer repeat units as commonly desired for photovoltaic applications.

Acknowledgment. We gratefully acknowledge funding of this work by the AFOSR (FA9550-09-1-0320) and Sestar, LLC.